ADVANCES IN ATMOSPHERIC SCIENCES, VOL. 30, NO. 3, 2013, 561–576

The Flexible Global Ocean-Atmosphere-Land System Model, Spectral Version 2: FGOALS-s2

BAO Qing[1] (包 庆), LIN Pengfei[1] (林鹏飞), ZHOU Tianjun*[1] (周天军), LIU Yimin[1] (刘屹岷), YU Yongqiang[1] (俞永强), WU Guoxiong[1] (吴国雄), HE Bian[1] (何 编), HE Jie[1] (何 杰), LI Lijuan[1] (李立娟), LI Jiandong[1] (李剑东), LI Yangchun[1] (李阳春), LIU Hailong[1] (刘海龙), QIAO Fangli[2] (乔方利), SONG Zhenya[2] (宋振亚), WANG Bin[1] (王 斌), WANG Jun[1] (王 军), WANG Pengfei[1] (王鹏飞), WANG Xiaocong[1] (王晓聪), WANG Zaizhi[3] (王在志), WU Bo[1] (吴 波), WU Tongwen[3] (吴统文), XU Yongfu[1] (徐永福), YU Haiyang[1] (于海洋), ZHAO Wei[2] (赵 伟), ZHENG Weipeng[1] (郑伟鹏), and ZHOU Linjiong[1] (周林炯)

[1]*State Key Laboratory of Numerical Modeling for Atmospheric Sciences and Geophysical Fluid Dynamics, Institute of Atmospheric Physics, Chinese Academy of Sciences, Beijing* 100029

[2]*First Institute of Oceanography, State Oceanic Administration, Qingdao* 266061

[3]*Beijing Climate Center, China Meteorological Administration, Beijing* 100081

(Received 10 June 2012; revised 12 November 2012)

ABSTRACT

The Flexible Global Ocean-Atmosphere-Land System model, Spectral Version 2 (FGOALS-s2) was used to simulate realistic climates and to study anthropogenic influences on climate change. Specifically, the FGOALS-s2 was integrated with Coupled Model Intercomparison Project Phase 5 (CMIP5) to conduct coordinated experiments that will provide valuable scientific information to climate research communities. The performances of FGOALS-s2 were assessed in simulating major climate phenomena, and documented both the strengths and weaknesses of the model. The results indicate that FGOALS-s2 successfully overcomes climate drift, and realistically models global and regional climate characteristics, including SST, precipitation, and atmospheric circulation. In particular, the model accurately captures annual and semi-annual SST cycles in the equatorial Pacific Ocean, and the main characteristic features of the Asian summer monsoon, which include a low-level southwestern jet and five monsoon rainfall centers. The simulated climate variability was further examined in terms of teleconnections, leading modes of global SST (namely, ENSO), Pacific Decadal Oscillations (PDO), and changes in 19th–20th century climate. The analysis demonstrates that FGOALS-s2 realistically simulates extra-tropical teleconnection patterns of large-scale climate, and irregular ENSO periods. The model gives fairly reasonable reconstructions of spatial patterns of PDO and global monsoon changes in the 20th century. However, because the indirect effects of aerosols are not included in the model, the simulated global temperature change during the period 1850–2005 is greater than the observed warming, by 0.6°C. Some other shortcomings of the model are also noted.

Key words: FGOALS, FGOALS-s2, ESM, CSM, CMIP5

Citation: Bao, Q., and Coauthors: The Flexible Global Ocean-Atmosphere-Land System model, Spectral Version 2: FGOALS-s2. *Adv. Atmos. Sci.*, **30**(3), 561–576, doi: 10.1007/s00376-012-2113-9.

1. Introduction

The climate system consists of five major interacting components: the atmosphere, the hydrosphere, the cryosphere, the land surface, and the biosphere. Addressing the interplay of different components and establishing the climate system's response to changes in anthropogenic emissions of greenhouse gases require

*Corresponding author: ZHOU Tianjun, zhoutj@lasg.iap.ac.cn

a coupled climate-system approach. Recognizing the central importance of climate models in climate studies, the Institute of Atmospheric Physics (IAP), Chinese Academy of Sciences has focused a great deal of effort on the development and application of numerical climate models, as part of the research activities of the State Key Laboratory of Numerical Modeling for Atmospheric Sciences and Geophysical Fluid Dynamics (LASG). Many pioneering Chinese climate models, including the Flexible Global Ocean-Atmosphere-Land System model, Spectral Version 2 (FGOALS-s2) described in this paper, have been developed at LASG-IAP.

The FGOALS-s2 is a global climate system model developed by researchers mainly from the LASG-IAP. The FGOALS-s2 was developed to provide a powerful numerical tool for realistically simulating climate, modeling anthropogenic influences on climate change, and understanding the processes and mechanisms of climate variability. The model has been available to many scientific communities for the solution of climate-related problems occurring at a broad range of timescales, from diurnal to centennial and even millennial. The FGOALS-s2 has been useful for Chinese climate research on topics such as paleo-climate, historical climate, recent global warming, and future climate projection.

The early version of FGOALS-s2, the Global Ocean-Atmosphere-Land System model (GOALS), a first-generation air-sea coupled model of the LASG/IAP, was released at the end of the 20th century (Zhang et al., 2000). The first spectral version of the Flexible Global Ocean-Atmosphere-Land System model (FGOALS-s1) was released in 2004. Compared with GOALS, the spatial resolution of each component of FGOALS-s1 was markedly increased, from 5° to 2.81° longitude and 4° to 1.66° latitude (Liu et al., 2004; Wang et al., 2005), and the models of several major physical processes were improved (Zhou et al., 2005). In 2010, the atmosphere component of the LASG IAP climate system model was updated to Spectral Atmospheric Model of IAP LASG, version 2 (SAMIL2); the relevant coupled model was named FGOALS-s1.1. The major modifications of this coupled model were in the atmospheric components involving the radiation scheme, the cumulus parameterization scheme, and the cloud scheme (Bao et al., 2010).

FGOALS-s2 is the newest member of the FGOALS-s family; this version has been used in the Coupled Model Intercomparison Project Phase 5 (CMIP5) experiments. The standard format results of FGOALS-s2 were submitted to CMIP5 via a network of servers called Earth System Grid data nodes. This overview paper describes the main developments and improvements in the model components. The performance of the model in simulating mean climate and major climate phenomena is assessed, and its strengths and weaknesses are documented.

The paper is organized as follows. The framework of the model and experimental designs are documented in section 2; section 3 is a presentation of simulated results of model stability, time-mean characteristics, and patterns of atmospheric circulation variability; finally, section 4 provides a conclusion and discussion.

2. Model descriptions and experimental designs

The climate system model version of FGOALS-s2 includes four individual components: an atmosphere component, SAMIL2 (Bao et al., 2010; Liu et al., 2013); an ocean component, the LASG IAP Climate System Ocean Model version 2 (LICOM2) (Liu et al., 2013); a land component, the Community Land Model version 3 (CLM3) (Oleson et al., 2004); and a sea ice component, the Community Sea Ice Model version 5 (CSIM5) (Briegleb et al., 2004). A flux coupler module (Collins et al., 2006) drives these four major components.

The major differences between FGOALS-s1.1 and FGOALS-s2 are the ocean component, the land component, the sea ice component and the coupler, which are updated in FGOALS-s2, while the atmosphere component still shares the same resolution and physical modules with FGOALS-s1.1 (Bao et al., 2010).

2.1 *The atmosphere component and the land component*

The atmospheric component of FGOALS-s2, SAMIL2 version 2.4.7, is a spectral model with a horizontal resolution of R42, approximately 1.66° (lat)×2.81° (lon). There are 26 vertical layers and the top layer of SAMIL2 is 2.19 hPa, except for radiation processes, 10-minute dynamic and physical time increment of integration in the SAMIL2 is employed. The radiation scheme in SAMIL2 is the Sun-Edwards-Slingo scheme (Edwards and Slingo, 1996; Sun and Rikus, 1999a, b; Sun, 2011); the scheme is able to accommodate the direct effects of aerosols (Li et al., 2012). The cumulus parameterization of SAMIL2 is the mass flux scheme of Tiedtke (1989) (Song, 2005). The planetary boundary layer (PBL) component is a higher-order closure scheme (Brinkop and Roeckner, 1995).

The land component of FGOALS-s2 is CLM version 3.0 (Oleson et al., 2004), while CLM version 2 is used in FGOALS-s1.1. The land component has a hor-

izontal resolution of 1.66° (lat) and 2.81° (lon), which are the same as those of the atmospheric component. The details of CLM3 can be found in the Technical Description of the Community Land Model in Oleson et al. (2004). The CLM3 is able to use a flexible time step. In our CMIP5 runs, a time step of 20 minutes was employed.

2.2 *The ocean component and the sea ice component*

The oceanic component of FGOALS-s is LICOM, which is the fourth generation of the LASG Oceanic General Circulation Model (OGCM) (Liu et al., 2004); the first generation was introduced in 1989 (Zhang and Liang, 1989). FGOALS-s2 uses LICOM2 that contains several improvements relative to LICOM1.0 and LICOM1.1, which is used in FGOALS-s1.1. First, the horizontal resolution in LICOM2 has been increased in the tropics (from 1°×1° to 0.5°×0.5°) and the vertical resolution has been adjusted to 10-m layer thicknesses in the upper 150 m (Wu et al., 2005). Second, a new advection scheme has been introduced in LICOM2 (Xiao, 2006). Third, the modeling of physical processes has been updated or improved, including those for mixing schemes (Canuto et al., 2001; Liu et al., 2013) and the solar penetration scheme (Lin et al., 2007).

The sea ice component of FGOALS-s2 is CSIM5 (Briegleb et al., 2004), which is a thermodynamic-dynamic sea ice model. CSIM5 is an updated version of CSIM version 4, while the version 4 is used in FGOALS-s1.1. The CSIM5 shares the same grid system as that of the ocean component, which is required by the flux coupler component of FGOALS-s2.

2.3 *FGOALS-s2 CMIP5 experiments*

CMIP5 standard experiments included two suites of runs: (1) long-term experiments performed at century-long time scales, and (2) near-term experiments performed at decadal time scales. Runs at both time scales were grouped as either "core" set, "tier 1" set, or "tier 2" set, based on the experiments' prioritization: the core experiments are taken as basic runs, which should be completed by all models. The tier 1 experiments are taken as the first priority runs, which are about specific aspects of climate model forcing, response, and processes, and tier 2 experiments are more specific aspects than tire 1 experiments (Taylor et al., 2012). All "core" experiments, most supplemental "tier 1" experiments, and some "tier 2" experiments conducted at both time scales have been successfully performed using FGOALS-s2. In terms of long-term experiments, FGOALS-s2 has been integrated over a period of more than 2700 model years, generating a total of approximately 40 terabytes of output data.

In this study, both pre-industry control experiments and 19th–20th century simulations (historical simulations) were used to evaluate model output of FGOALS-s2 CMIP5 long-term runs. The pre-industry control experiment has been integrated over a period of more than 1000 years, and the last 500 years of data were submitted to CMIP5. All varieties of forcing in the pre-industry control run were fixed at the year 1850. The historical simulations were integrated over the period 1850–2005. The historical simulations include imposed changes in atmospheric composition (including CO_2), caused by volcanic influences, solar radiative forcing, concentrations of short-lived atmospheric species, and concentrations of natural and anthropogenic aerosols. To reduce the uncertainties arising from different initial conditions, three groups of historical simulations were performed as ensemble members; the initial conditions of these runs were different from those of the pre-industry experiment. The following evaluations and diagnoses were retrieved from the three ensemble means, and the time means from 1971 to 2000 were then treated as climatological results. To investigate variations in patterns of atmospheric circulation, the analyses were performed for all ensemble members, but only the results from the first ensemble member are reported in this paper.

3. Results

3.1 *Stability*

The stability of a climate system model is a critical criterion, guaranteeing for the achievement of long-term integration; usually, time series of global mean SST obtained from model control runs are taken as an important index for quantifying the coupled model's stability. The time series of the annual global-mean SST (Figure not shown) was derived from the 500-year pre-industry control run of FGOALS-s2. Variabilities at multiple time scales, from interannual to interdecadal, in the climate system can be detected by the SST index, while an insignificant trend of −0.1°C per 500 years was observed in a long-term control run. The long-term trend of the SST index reflects the stability of mass and energy flux exchanges at the air-sea interface. Additionally, some other important indexes, including the mass, water content, sea ice, salinity, and global ocean heat transport etc., have been examined to check the stability, they share the same results of SST (Lin et al., 2013). In this regard, FGOALS-s2 successfully exhibits stability with respect to air-sea coupling.

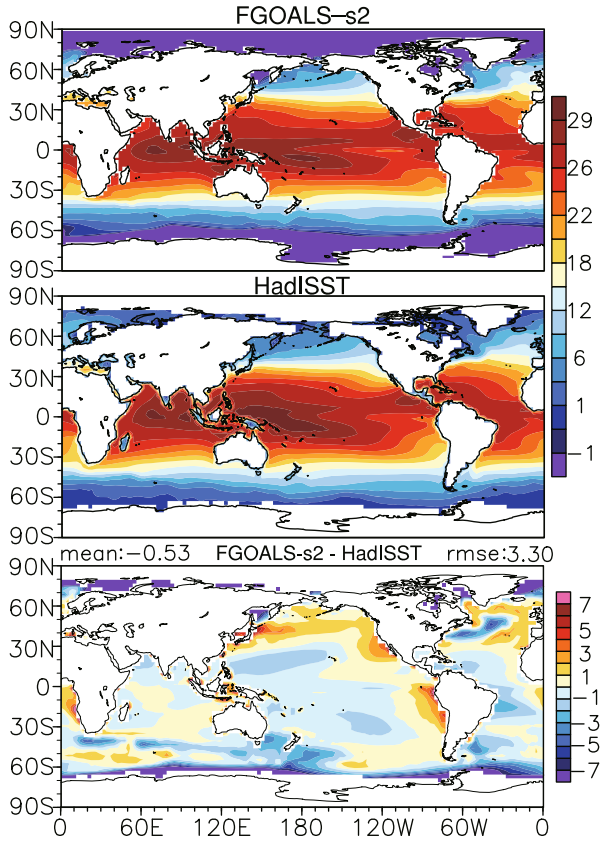

Fig. 1. Annual mean Sea Surface Temperature for the model (top), the observation (middle) and their difference(bottom). Hadley Centre sea-Ice and Sea Surface Temperature dataset [HadISST (Rayner, et al., 2003)] is used for comparison as the observation. Units: °C.

3.2 *Time-mean characteristics*

3.2.1 *Ocean and sea ice climatology*

Global distribution of annual mean SST was used to address model behavior and drift; these were retrieved from the three ensemble runs of the FGOALS-s2 historical experiments. The general characteristics of tropical SSTs show a warm pool in the Western Pacific and Indian Ocean and a cold tongue in the Eastern Pacific. The modeling results were compared with values from the Hadley Centre sea-Ice and Sea Surface Temperature dataset (HadISST) (Rayner et al., 2003), which are taken as the observed SSTs (see Fig. 1). Although the northward extension of the western Pacific warm pool is slightly underestimated, FGOALS-s2 fairly simulates the main characteristics of the warm pool SST in both the equatorial Indian Ocean and the equatorial western Pacific; in particular, the model successfully captures the two warm (29°C) SST centers along the equatorial Indian Ocean. The successful simulation of the cold tongue provides a good solution for overcoming the modeling bias of the "double intertropical convergence zone (ITCZ)". The simulated cold tongue by the FGOALS-s2 is quite close to that of the observations, especially along the simulated 26°C SST contour in the equatorial Eastern Pacific, which, in the Southern Hemisphere (SH), extend approximately to 115°W longitude. Therefore, the phenomenon of the "double ITCZ" generally disappears. This conclusion is also supported by the simulated mean annual precipitation. However, the main biases in the simulation of SST are positive along the western coastlines of continents, including South America, North America, and Africa; these biases may be related to the less simulated stratus cloud over the off-equatorial East Pacific and Southern-east Atlantic margins regions (not shown), which leads to the strengthened downward shortwave flux, then induces the warm biases of SST in these regions. Overall, it is concluded that no significant climate drift exists in the simulations.

One of the highlights of the FGOALS-s2 is its performance in simulating the climatological mean annual cycle of equatorial Pacific SST. Figure 2 shows the climatological mean annual cycles of equatorial Pacific SST from the FGOALS-s2 and HadISST. FGOALS-s2 reasonably reproduces three distinct characteristics of the climatological mean annual SST cycles in this region, including the realistic annual cycle structure of equatorial Eastern Pacific SST, the realistic semi-annual cycle structure of equatorial Western Pacific SST, and their transition phases, which appear as a westward extension of the warm SST anomalies in the early parts of the year.

Ocean meridional circulations play an important role in transporting heat. Figure 3 shows global meridional overturning circulation (MOC) and Atlantic MOC (AMOC). The overall patterns and positions of cells, water masses, and overturning are similar to observed patterns (Lumpkin and Speer, 2007) and the results of other models (e.g., Meehl and Stocker, 2007). The tropics and subtropics cells in the upper layer (above 500 m) are mainly driven by wind stress. At depths of 500 to 2500 m North Atlantic Deep Water (NADW), which is mainly produced in the North Atlantic, dominates north of 35°S. The maximal value of NADW (19 Sv) is located at 26°N at a depth of approximately 1000 m, which is close to the observed value of 18.5 Sv at 26.5°N. Antarctic Bottom Water (AABW) is located north of 50°S at depths greater than 2500 m. At approximately 50°S, the Deacon cell penetrates from the surface to about 4000 m; its maximal value is 36 Sv. At high latitudes, polar MOCs exist in the SH and NH, with values of about 4 Sv in both regions. The further study suggests that the reasonable simulations of the oceanic mixed layer depth

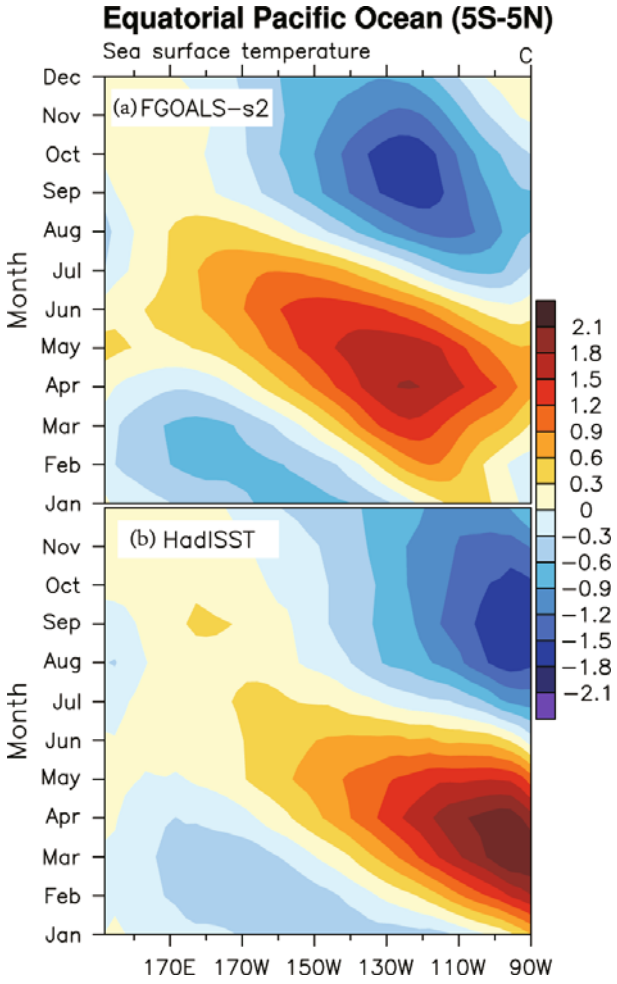

Fig. 2. Annual cycle of the equatorial Pacific SST in the model (a) and the observation (b). HadISST (Rayner et al., 2003) is used for comparison as the observation. The units of SST is °C. The equatorial Pacific Ocean regions is defined between −5°S to 5°N.

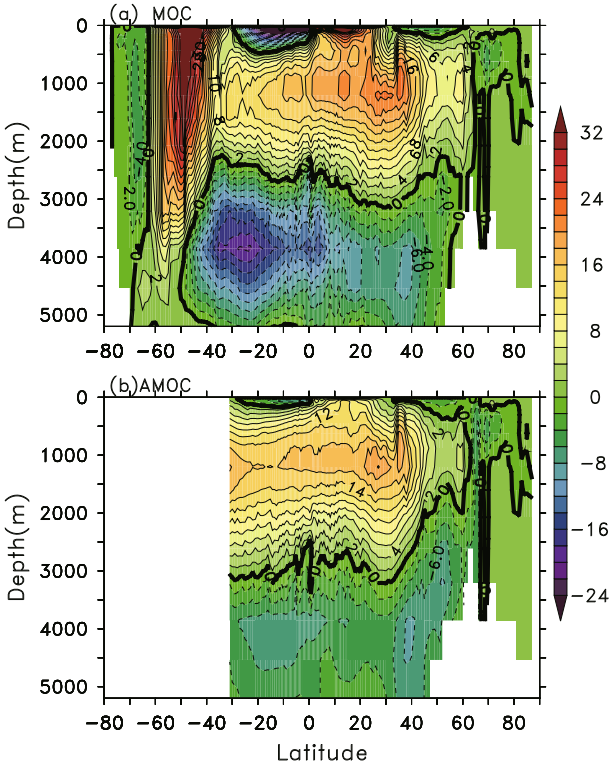

Fig. 3. The simulated Meridional Overturning Circulation (MOC) (a), and the Atlantic MOC (AMOC) (b) in FGOALS-s2. The units of MOCs is Sv, and the contour interval is 2Sv.

and the wind stirring lead to a realistic vertical mixing in FGOALS-s2, which enhances MOC and makes it more realistic compared with the results of FGOALS-s1 (Lin et al., 2013).

The mean annual sea ice concentrations in NH and SH are shown in Fig. 4. Since the enhanced MOC transports more heat from the tropics to middle and high latitude in FGOALS-s2, the sea ice concentrations become more realistic compared with FGOALS-s1's results (Lin et al., 2013). However, there are still some biases: the simulated extent of sea ice, as defined by 15% iso-contour lines, is less than observed (Fig. 4a) in Japan Sea, North Pacific, Bering Sea, Labrador Sea, and in downstream areas; while the sea ice concentration is overestimated in the Sea of Okhotsk, Norway Sea, and Barents Sea. These biases in the NH regions are mainly attributable to the simulated errors in March. In the SH regions, the maximal sea ice concentration is located in Weddle Sea, as observed (not shown). The extent of sea ice simulated by FGOALS-s2 (enclosed by the 15% concentration contour) is greater than observed, except in the Pacific and Indian Ocean regions, and the north of Weddle Sea (Fig. 4b). Additionally, the simulated seasonal variations are reported in another study (Lin et al., 2013).

3.2.2 *Atmosphere and land climatology*

The hydrologic cycle is a crucial component of the climate system. Figure 5 compares the global and zonal mean annual precipitation from FGOALS-s2 simulations with the Climate Prediction Center Merged Analysis of Precipitation observations (XIE-ARKIN) (Xie and Arkin, 1997). The FGOALS-s2 well reproduces the spatial patterns of precipitation along the ITCZ and the South Pacific convergence zone, although the precipitation center of the tropical Indian Ocean is shifted southeastward in the simulation. The annual, winter, and summer zonal means of precipitation from FGOALS-s2, the Global Precipitation Climatology Project (GPCP) (Adler et al., 2003), and CPC Merged Analysis of Precipitation (CMAP) are presented in Fig. 5. As compared with the two observa-

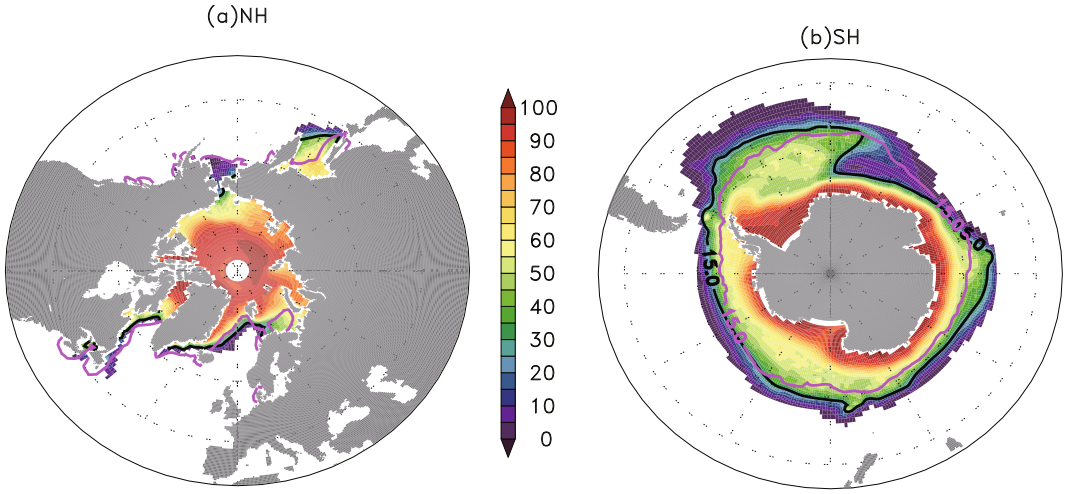

Fig. 4. The simulated annual mean sea ice concentrations (%) in Northern Hemisphere (a) and Southern Hemisphere (b) in FGOALS-s2. The purple red lines are for the observed 15%-concentration values. The black lines are for FGOALS-s2.

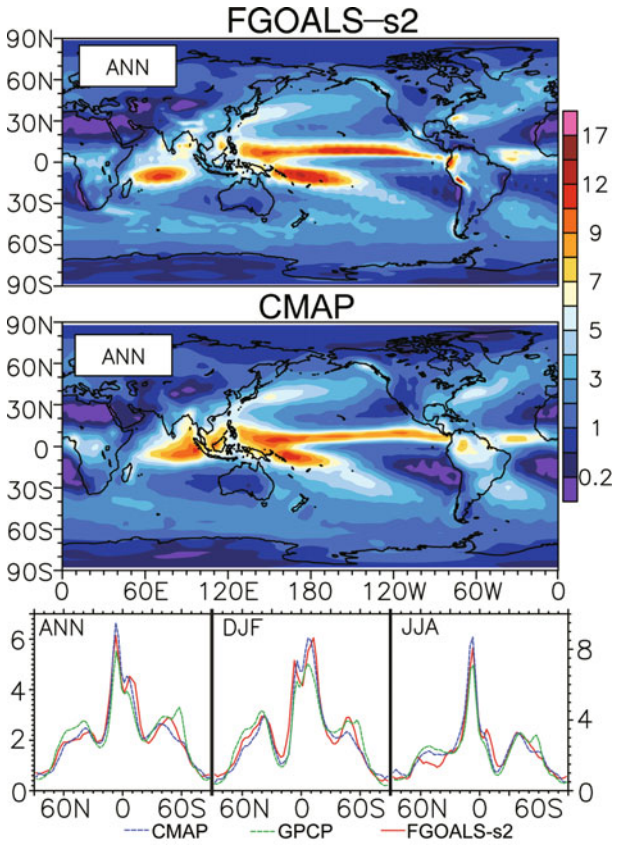

Fig. 5. Annual mean Precipitation in FGOALS-s2 (top) and XIE-ARKIN observations (middle) (Xie and Arkin, 1997); the lower panel is the zonal mean precipitation for Annual (ANN)(bottom left), December-January-February (DJF) (bottom middle) and June-July-August (JJA) (bottom right). The red solid lines are from FGOALS-s2, and the blue dashed lines are from XIE-ARKIN observations. Units: mm d^{-1}.

tional datasets, FGOALS-s2 well captures the local maximum peaks of precipitation in both tropical and subtropical regions, and realistically reproduces seasonal precipitation peaks, which are characterized by double peaks in the boreal winter with a maximum peak located in the SH and a single peak in the boreal summer with a maximum peak in NH. The global mean bias and RMS error between the model and CMAP observation are 0.03 mm d^{-1} and 1.21 mm d^{-1}.

Figure 6 shows the global annual mean values of the 2-meter air temperature (TAS) in the simulations of historical runs, as compared with the observation of CRU TS2.1 (Climatic Research Unit, University of East Anglia, Surface Temperature version 2.1: Mitchell and Jones, 2005). FGOALS-s2 well reproduces the basic patterns of the TAS, including warm continents in equatorial regions and cold continents close to Polar Regions. However, some biases are found in mid- to high latitude regions of NH, where FGOALS-s2 underestimates the lower TAS. Detailed analyses further suggest that the biases are strongly affected by the behavior of simulated low-level cloud amounts.

3.3 *Climate variability*

The evaluation of climate variability patterns simulated by FGOALS-s2 involves the following aspects: major teleconnection patterns, the ENSO, and the Pacific Decadal Oscillation (PDO). These aspects were compared with the observational data following the study in IPCC Fourth Assessment Report Chapter 3.6 (IPCC, 2007). The evaluation of the intraseasonal variability has been comprehensively reported in other

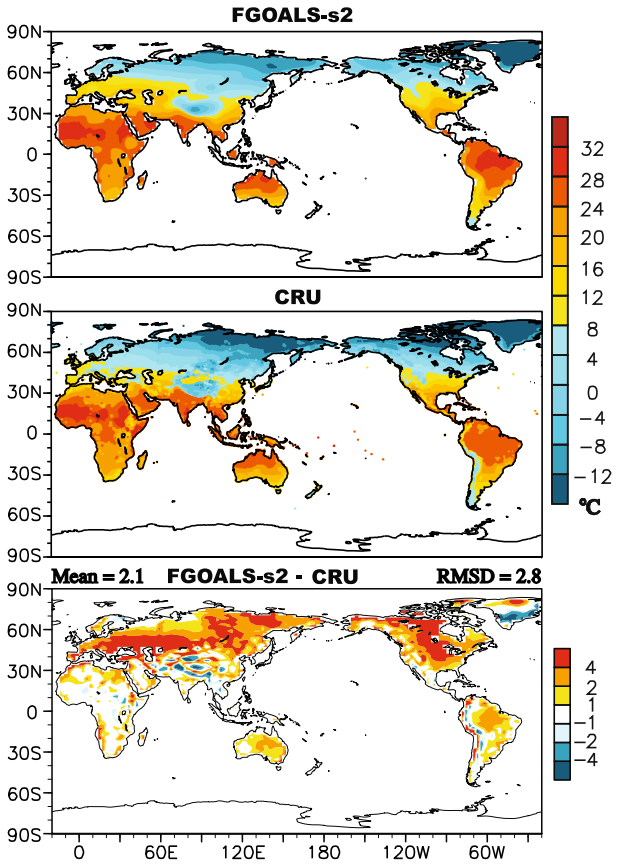

Fig. 6. Annual mean of the 2 meter air temperature for FGOALS-s2 (top), observation (CRU TS 2.1, Brohan et al., 2006) (middle) and their difference (bottom). The air temperature is in units of °C.

studies (Yang et al., 2008, 2010, 2012).

3.3.1 *Teleconnections*

The North Atlantic Oscillation (NAO) is a large-scale alternation involving atmospheric masses, and it strongly influences regional climate, particularly in the Atlantic-European sector, and even in East Asia (Yu and Zhou, 2004). Evaluation of the performance of the coupled system in simulating the NAO is one of the important foci of the climate modeling community.

To examine the NAO simulation by FGOALS-s2, the December–January–February (DJF) average of Sea Level Pressure (SLP) and the first leading mode of the EOF analysis of SLP are compared with the simulation results (Fig. 7). The simulation results are similar to observed wintertime mean SLP patterns in the Atlantic sector of NH, although the simulated Azores High is stronger than that in the reanalysis data; these patterns are similar to those achieved using a previous version of the FGOALS model (Zhou et al., 2000). The Icelandic Low simulated by FGOALS-s2 is matched well with the reanalysis data, except that the action center is shifted slightly northwards in the simulation and the simulation intensity is stronger than that in the reanalysis data (Figs. 7a, b).

To assess the ability of FGOALS-s2 to reproduce the NAO pattern, an EOF analysis was conducted on the SLP anomaly over the North Atlantic sector (0°–90°N, 110°W–50°E). The leading EOF pattern of the DJF SLP derived from the simulation (Fig. 7d) shows a classic NAO signal, similar to that observed in the reanalysis data (Fig. 7c); both features show a seesaw-like variation in the DJF SLP between Iceland and Azores. The variances explained by the simulation and the reanalysis data are also comparable: the EOF1 of the reanalysis data accounts for 45.1% of the DJF SLP variability in the region, while the EOF1 of the FGOALS-s2 accounts for 43.8% of the variance. Thus, the FGOALS-s2 model produces a faithful simulation of the NAO.

The Pacific-North America (PNA) teleconnection is one of the most prominent large-scale patterns of atmospheric low-frequency variability in the northern extra-tropics, arching from the tropical Pacific across to North America; it is a good example of a wave train.

To measure the intensity of the PNA teleconnection, the PNA index (IPNA) defined in Wallace and Gutzler (1981) is used.

$$\mathrm{IPNA} = \frac{[Z^*(20^\circ\mathrm{N}, 160^\circ\mathrm{W}) - Z^*(45^\circ\mathrm{N}, 165^\circ\mathrm{W}) + Z^*(55^\circ\mathrm{N}, 115^\circ\mathrm{W}) - Z^*(30^\circ\mathrm{N}, 85^\circ\mathrm{W})]}{4}.$$

Where, for example, Z^*(20°N, 160°W) represents a normalized departure from the mean 500-hPa geopotential height at 20°N, 160°W in winter. In the reanalysis (Fig. 8), the regression coefficients are about 15 gpm over the subtropical North Pacific, close to 40 gpm over northwestern North America, about −80 gpm over the northeast Pacific, and about −20 gpm over southwestern North America. The four anomalous centers are located over the North Pacific and across North America, presenting a typical PNA teleconnection pattern. The spatial patterns of the PNA teleconnection derived from the reanalysis data are reasonably simulated by FGOALS-s2, but the simulated anomalous centers are generally stronger than their counterparts in the reanalysis data, except for the center over the subtropical North Pacific.

3.3.2 *ENSO variability*

On interannual time scales, the leading mode of global SST variability is related to ENSO events. The

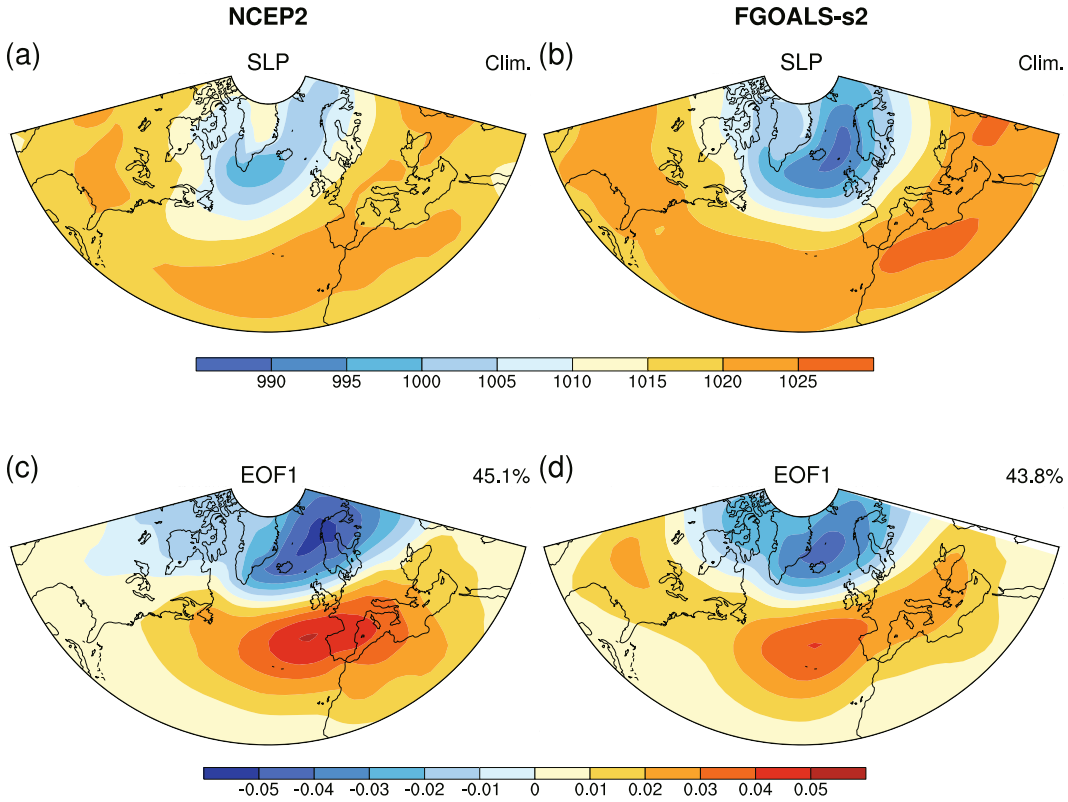

Fig. 7. The DJF averages of sea level pressure (SLP) (a, b, in hPa) and the first EOF modes of DJF SLP covariance matrices (c, d). (a, c) are based on NCEP2 reanalysis data for the period of 1979–2009. (b, d) are based on FGOALS-s2 historical run 1971–2000.

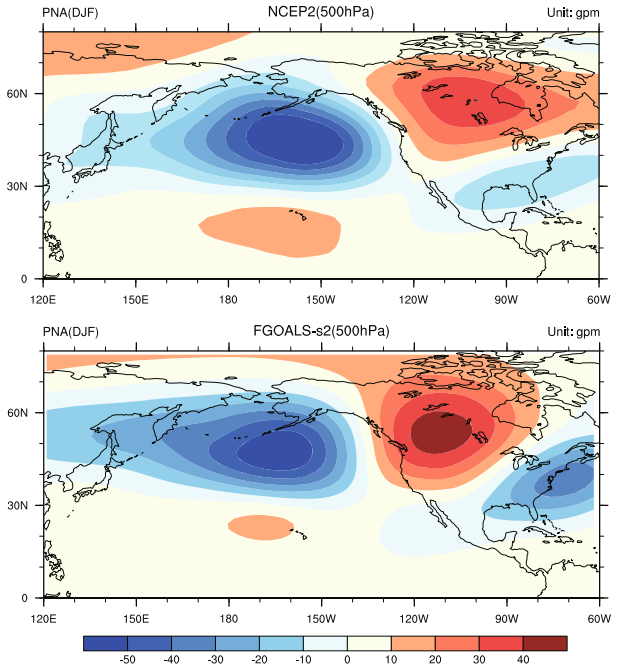

Fig. 8. Regression coefficients of winter 500 hPa geopotential height anomaly from NCEP2 (top) data, and FGOALS-s2 (bottom) Historical run against the corresponding PNA index. Units: gpm.

method of EOF is used to retrieve the leading mode of SST from the coupled models and observations. As illustrated in Fig. 9, FGOALS-s2 shows a remarkable reproduction of the spatial pattern of the leading mode of SST, but the simulated negative SST anomalies over the south and north Pacific regions are a little weaker than observed anomalies. It should be noted that the simulated negative correlation associated with the PNA pattern over North Pacific is weaker than the observed values (Fig. 8), which implies a weaker response of the atmosphere in middle latitudes to tropical thermal forcing; this is also demonstrated by the correlation coefficients between the PNA index and the Niño3 index, which are −0.4 and −0.2 for the observations and the model, respectively. As a result of the weaker response to tropical heating, the negative SST anomalies associated with ENSO events in the North and South Pacific are weaker than those observed in Fig. 9. On the other hand, FGOALS-s2 successfully simulates a characteristically broad spectral peak in the range of two–seven years with double peaks at around four and six years, which is basically consistent with Reynolds observations, although the model simulates a slightly longer period for the ENSO than what is observed. Furthermore, the correspond-

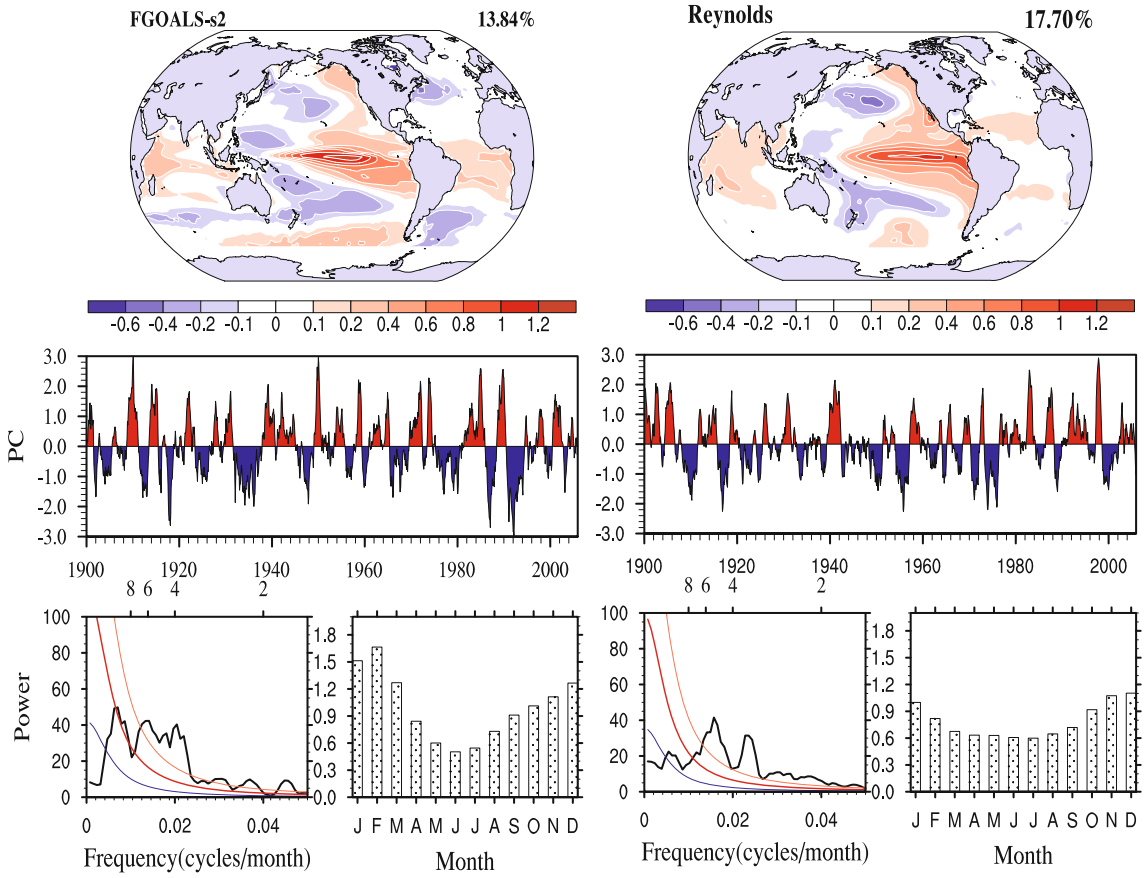

Fig. 9. The leading mode of global SST Variability in FGOALS-s2 (left) and Reynolds (right). The empirical orthogonal analysis (EOF) is used to get the leading mode of SST. The corresponding principal component (PC) are shown in the middle panels. The lower panels are the spectral analysis on the PC (bottom curves) and the variance of the PC (bottom bars) for the FGOALS-s2 (bottom left) and Reynolds (bottom right). In the bottom curve figures, the red lines are the "Markov red noise", and orange and blue lines represent the 95% and 5% significance levels respectively.

ing time series show a phase-lock phenomenon similar to what is observed; e.g., the largest SST anomalies associated with simulated ENSO events occur in boreal winter. Compared with previous versions of FGOALS (Yu et al., 2011), the prominent improvements in the current version are in the simulations of the ENSO's amplitude and irregularity. The standard deviation of the observed Niño3 index is approximately 0.85°C; FGOALS-s2 produces a very close estimate, of 0.88°C.

3.3.3 *Pacific Decadal Oscillation*

The PDO, the leading mode of SST anomalies in the North Pacific, represents a coupled mode of the ocean-atmosphere system; thus the PDO signal can be found in subsurface ocean and atmospheric circulation patterns. The time series of the first EOF for SST anomalies for models and observations in the North Pacific are shown in Fig. 10; both patterns show prominent decadal variability. The spatial pattern of the PDO is derived by a regression of the first principal component against global SST anomalies. The observed spatial PDO pattern is very similar to that of ENSO, e.g., showing positive anomalies in the tropical Pacific and negative anomalies in the North Pacific, although the latter is stronger than the former in the PDO pattern, and the former is stronger than the latter in the ENSO pattern, as noted by Zhang et al. (1997). The PDO pattern in the simulations is fundamentally similar to the observed patterns, in that there is a negative correlation between SST anomalies in the tropical and North Pacific in both the observed and simulated data, but positive anomalies in the tropical Pacific are much weaker in the simulations than in the observed data. Thus, at decadal and interdecadal time scales, the simulated relationship between the tropical and North Pacific is weaker than observed, which is similar to what is found at interannual time scales. Because the PDO signal can be regarded as a

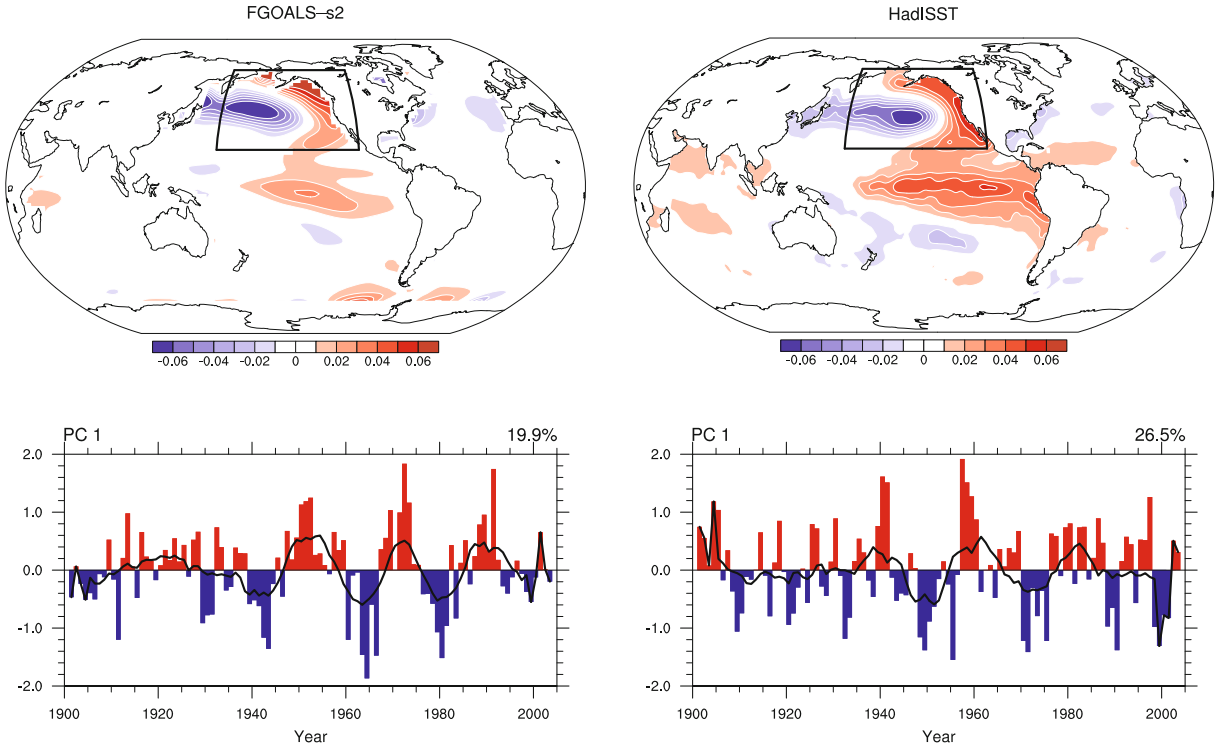

Fig. 10. Pacific Decadal Oscillation in FGOALS-s2(left panels) and HadISST (right panels). SST based on the leading EOF SST pattern for the North Pacific basin (20°–65°N, 160°E–110°W) from 1901 to 2004 (top panels); time series of the first EOF mode of SST anomalies in the box shown (standardized), and the solid black curve shows decadal variations after 10-year run-average. (bottom panels).

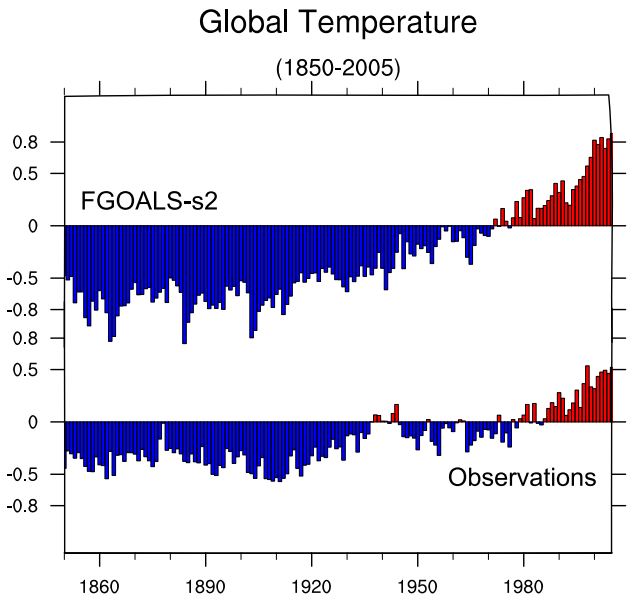

Fig. 11. The time series of the global mean 2m air temperature from 1850 to 2005. FGOALS-s2 is on the top, and HadCRUT3v observation is on the bottom. Units: °C.

residual effect of ENSO variability (Zhang et al., 1997), the cause of the model bias in the PDO pattern should be similar to that in ENSO—the simulated atmospheric response to El Niño warming is weaker than observations in North Pacific.

3.4 *19th–20th century climate*

The global means of surface temperatures from FGOALS-s2 simulations and HadCRUT3v (variance adjusted version of HadCRUT3) observations (Brohan et al., 2006) are shown in Fig. 11; the correlation coefficient between these two time series is 0.873. The HadCRUT3v observations exhibit two major warm-climate periods during the period 1850–2005, which are denoted by red bars at the bottom of Fig. 11. FGOALS-s2 successfully captures the later warm-climate period, starting in the 1970s, while the model failed to simulate the first warm-climate period that occurred in the 1940s. The global surface temperature based on HadCRUT3v has increased 0.7°C since the late 19th century (1850–2005), but the simulated global surface temperature in FGOALS-s2 historical runs has increased 1.3°C. Thus, the simulated warm-amplitude of FGOALS-s2 is greater than that of the HadCRUT3v data, which is likely due to a miss-

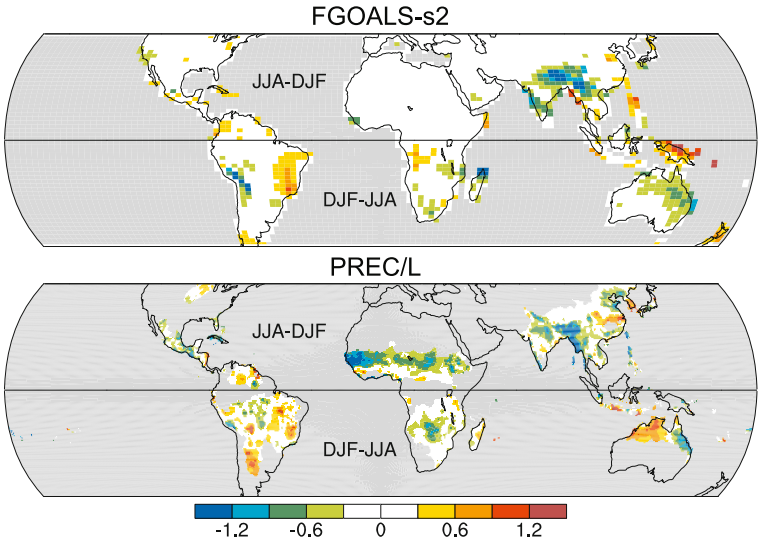

Fig. 12. Changes in the mean annual range of precipitation in FGOALS-s2 (top) and PREC/L (Chen et al., 2002) (bottom): 1978 to 2004 minus 1951 to 1977 periods (mm d^{-1}). Blue/green (red/yellow) color denotes a decreasing (increasing) annual range of the monsoon rainfall. Grey areas indicate missing values (oceans) or areas with insignificant annual changes. Data were from GPCC and passed 90% *t*-test are plotted.

ing component in the model for the indirect effects of aerosols.

Hydrologic changes in the 20th century climate are explored through changes in the mean annual range of precipitation, which is attributed to the global monsoon (Wang and Ding, 2006). Figure 12 shows the changes in the mean annual range of precipitation from FGOALS-s2 simulations and PREC/L (NOAA's PRECipitation REConstruction over Land) observations (Chen et al., 2002), and the differences between the changes during the period 1976–2003 and those during the period 1948–75. As compared with observational changes, FGOALS-s2 well captures the weakening trends of the South Asian monsoon, the East Australian monsoon, and the South African monsoon, and the strengthening trend in the eastern part of the South American monsoon. However, the simulation does not capture the drying and moistening trends in the regions of the North African monsoon and East Asian monsoon. In addition, the model fails to reproduce the drying trends in the monsoon regions of the southern U.S. and northern China.

3.5 *Monsoon simulations*

3.5.1 *Asian monsoon*

The Asian monsoon, the most powerful monsoon system in the world, includes the South Asian summer monsoon (SAM), the East Asian summer monsoon (EASM), and the western North Pacific summer monsoon (WNPSM). Observed Asian monsoon precipitations and circulations are shown in Fig. 13a. The five major South Asian tropical precipitation centers are located on the western rim of India and in the Bay of Bengal, the South China Sea, the Philippine Sea, and the southeastern Indian Ocean to the west of Sumatra. In the subtropical zone, a substantial Meiyu rainband extends eastward from the middle and lower reaches of the Yangzi River to the east of Japan. A strong cross-equatorial Somalia jet in the western Indian Ocean corresponds to precipitation distributions in this area; the stream turns eastward from the Arab Sea to the South China Sea, and then turns northward and transfers water vapor poleward.

The FGOALS-s2 reproduces the five major tropical precipitation centers, although the simulated precipitation on the western rim of India is stronger than observed values, while the simulated precipitation in South China Sea and western North Pacific is much weaker than observed values. Meanwhile, the model gives unrealistic precipitation levels on the southern slope of Tibetan Plateau. The ITCZ in the southern tropical Indian Ocean simulated by FGOALS-s2 is shifted westward and poleward relative to that in the observations. Correspondingly, the cross-equatorial component of the Somalia Jet is weak in the FGOALS-s2 simulation. In the subtropical zone, the simulated Meiyu rainband is shifted outside of East Asia; the discrepancy is associated with the eastward withdrawal

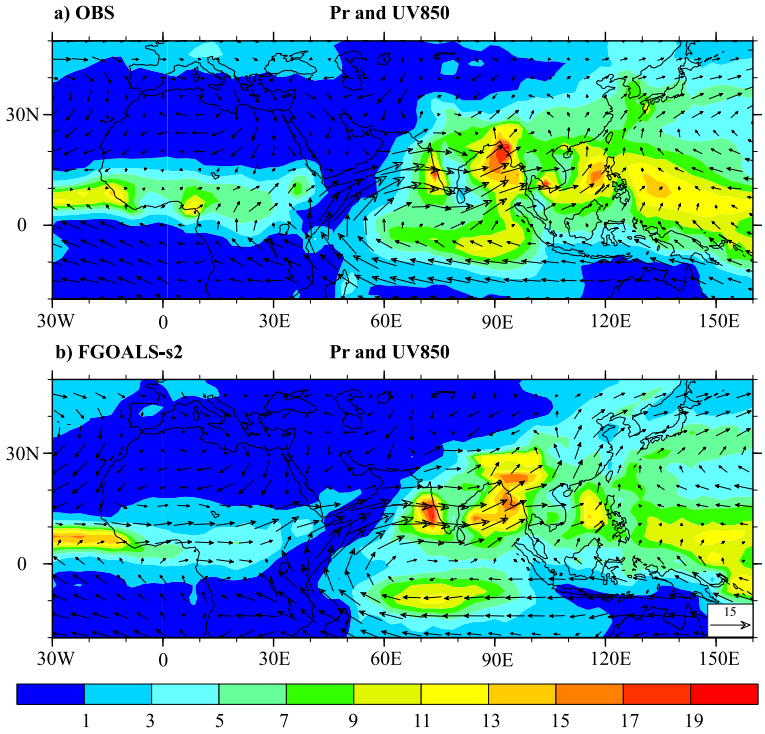

Fig. 13. The boreal summer mean of precipitation (color shading in unites of mm d^{-1}) and 850 hPa winds (vectors in units of m s^{-1}) in observation (wind is from NCEP2 and precipitation is from CMAP datasets) (a) and FGOALS-s2 (b).

of the western edge of the western Pacific subtropical high.

The stepwise meridional displacement is one of the most distinctive characteristics of the East Asian monsoon, as compared with other tropical monsoon systems. Observations show that the main rainband, located in South China before mid-May (Fig. 14), reaches the middle and lower reaches of the Yangzi River in June, during which time it forms the Meiyu frontal zone. The monsoon precipitation expands to its northernmost extent (at about 40°N) in July and August, and gradually withdraws southward thereafter. The FGOALS-s2 reproduces the stepwise meridional displacement of the monsoon rainband, although the simulated southward withdrawal of the rainband is slower than that of the observed withdrawal (Fig. 14).

3.5.2 *African monsoon*

The African monsoon is mainly caused by the thermal contrast between African Continent and Atlantic Ocean, and the monsoon rainbelt follows seasonal movement of the ITCZ. The surface air temperature gradient and the sea level pressure are reasonably simulated by FGOALS-s2, in particular, the vertical extension and magnitude of the dry convection in the African heat low is well captured in North Africa (Figure not shown). FGOALS-s2 reproduces a belt of maximum precipitation between 5°N and 10°N (Fig. 13b), which is consistent with observations. However, the rainfall maximum along the Gulf of Guinea is not well captured, and the total precipitation over land is underestimated by the model. The seasonal movement of the monsoon rainbelt broadly follows the observation, but the timing is delayed by one month (Fig. 14d). Although the northern limit of ITCZ movement is about 5° northward more than that in the observation, the monsoonal precipitation is underestimated particularly during the boreal summer (Fig. 14b). The zonal averaged profile of the vertical velocity shows that simulated convection within the ITCZ is weaker than that in NCEP2 reanalysis data (Figure not shown), which leads to a simulated weaker total precipitation (Figs. 13b and 14d).

4. Summary and conclusions

This study described the framework and performances of the global climate system model named FGOALS-s2. The FGOALS-s2 consists of: SAMIL2, the atmosphere component; LICOM2, the ocean component; CSIM5, the sea ice component; and CLM3, the land component. These components are cou-

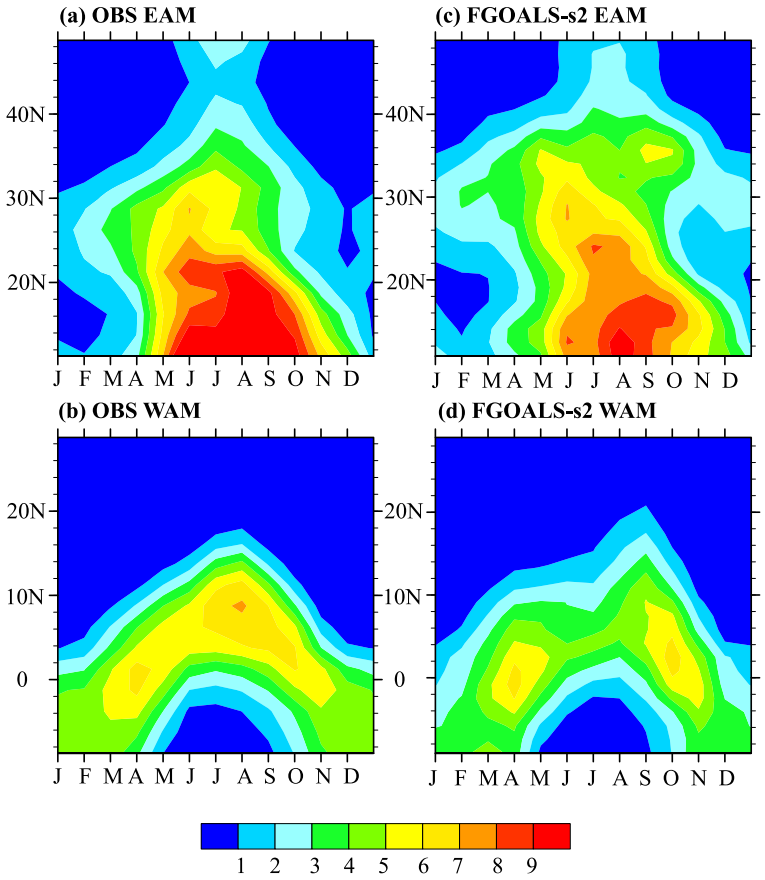

Fig. 14. Annual cycle of zonal mean precipitation for East Asian Monsoon (110°–120°E) (a, c), Western African Monsoon (10°W–30°E) (b, d). (a) and (b) are from CMAP, (c) and (d) are from FGOALS-s2. Units: mm d^{-1}.

pled together with the flux coupler from NCAR. FGOALS-s2 has been used to conduct the experiments for analysis studies supporting the IPCC AR5 and the CMIP5. The 500-year pre-industry control run and three groups of 19th–20th historical runs were adopted in this study to exhibit the general behaviors of FGOALS-s2.

In conclusion, the FGOALS-s2 exhibits significant improvements and stability in the long-term control run, for reproducing climatological time-mean behaviors, and for simulating patterns of atmospheric circulation variability. The comprehensive evaluations indicate that climate drift is well controlled. The FGOALS-s2 simulates a realistic global climate: the model shows reasonable warm pools and cold tongue, the common bias of the 'double ITCZ' is greatly reduced, and the simulated precipitation is comparable with observations. Meanwhile, the behaviors of the simulated ASM and the annual cycle of rainfall in East Asia are reasonable. In particular, the model well captures the phenomena of annual and semiannual cycles of SST in the equatorial Pacific Ocean. The simulated patterns of atmospheric circulation variability are further examined using the PNA and NAO teleconnections, ENSO-related modes of global SST, PDO, and 19th–20th century climate. The comparisons between simulations and observations indicate that FGOALS-s2 pretty well reproduces the main characteristics of PNA and NAO teleconnections, ENSO irregular periods, and the global response to ENSO signal; the simulations of both PDO and the global monsoon changes in the 20th century are fairly reasonable.

FGOALS-s2 also shows some biases, and our model team members are working towards eliminating these biases. The major bias in the climate change simulation is that the global mean warming amplitude for 19–20th century is slightly higher than observation. The absence of a component for the indirect effects of aerosols is probably a major cause of this bias. Fortunately, work is underway to develop a new approach that considers the indirect effects of aerosols, for incorporation into SAMIL2; thus, the indirect effects of

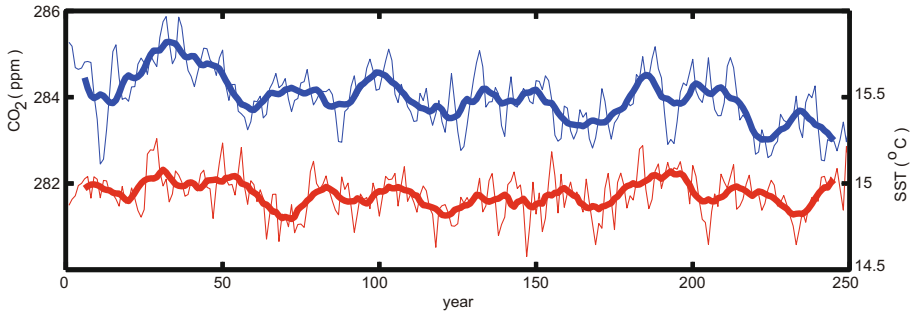

Fig. 15. Time series of the carbon dioxide (CO_2) concentrations (blue curves) and SST (red curves) in 250-year pre-industry control run with the earth system version of FGOALS-s2. The thick curves are smoothed by 11-year running mean. The trends of CO_2 is -1 ppm per 250 years and SST is -0.03°C per 250 years.

aerosols will be taken into consideration in the next version of FGOALS-s, which will refine the climate change simulation of FGOALS-s and may generate a more realistic result.

It has been pointed out that the incorporation of carbon cycle processes into the climate system model would make the climate changes of the model more realistic (Friedlingstein et al., 2006). The determination of the carbon feedback influence on climate change is of great interest for IPCC AR5 and CMIP5 models. The carbon cycle is included in both the land and ocean components of FGOALS-s2; namely, in the Earth System Model version (ESM) of FGOALS-s2, which is available for carbon–climate feedback study in CMIP5. In the ESM of FGOALS-s2, the land carbon processes are calculated using the Vegetation Global Atmosphere and Soil model of (VEGAS) (Zeng et al., 2004), and the ocean carbon cycle with a simple biogeochemical process is incorporated into the ocean component (LICOM) of the FGOALS-s2. This version of ocean carbon-cycle module (IAP-OBM) is a modified one that originated from the carbon cycle model of the Pacific Ocean (IAP-OBM) (Li and Xu, 2012). The preliminary results from the FGOALS-s2 ESM are given in Fig. 15, which shows the time series of CO_2 concentrations and corresponding SST for the 250-year pre-industry control run. The results demonstrate that both the carbon cycle and the coupled climate system reach stable states. Further studies with the FGOALS-s2 ESM will be reported soon.

Acknowledgements. This study was supported by "973" programs (Grant Nos. 2012CB417203, 2013CB955803 and 2010CB950404), "863" program (Grant No. 2010AA012305), CAS Strategic Priority Research Program (Grant No. XDA05110303), and the National Natural Science Foundation of China (Grant Nos. 41023002 and 40805038)

REFERENCES

Adler, R. F., and Coauthors, 2003: The version 2 global precipitation climatology project (GPCP) monthly precipitation analysis (1979–present). *Journal of Hydrometeorology*, **4**, 1147–1167.

Bao, Q., G. X. Wu, Y. M. Liu, J. Yang, Z. Z. Wang, and T. J. Zhou, 2010: An introduction to the coupled model FGOALS1.1-s and its performance in East Asia. *Adv. Atmos. Sci.*, **27**, 1131–1142, doi: 10.1007/s00376-010-9177-1.

Briegleb, B. P., C. M. Bitz, E. C. Hunke, W. H. Lipscomb, M. M. Holland, J. L. Schramm, and R. E. Moritz, 2004: Scientific description of the sea ice component in the community climate system model, version three. NCAR Tech. Note NCAR/TN-463+STR, 70pp.

Brinkop, S., and E. Roeckner, 1995: Sensitivity of a general circulation model to parameterizations of cloud-turbulence interactions in the atmospheric boundary layer. *Tellus A*, **47**, 197–220.

Brohan, P., J. J. Kennedy, I. Harris, S. F. B. Tett, and P. D. Jones, 2006: Uncertainty estimates in regional and global observed temperature changes: a new dataset from 1850. *J. Geophys. Res.*, **111**, doi: 10.1029/2005JD006548.

Canuto, V. M., A. Howard, Y. Cheng, and M. S. Dubovikov, 2001: Ocean turbulence. Part I: One-point closure model-momentum and heat vertical diffusivities. *J. Phys. Oceanogr.*, **31**, 1413–1426.

Chen, M., P. Xie, J. E. Janowiak, and P. A. Arkin, 2002: Global land precipitation: A 50-yr monthly analysis based on gauge observations. *Journal of Hydrometeorology*, **3**, 249–266.

Collins, W. D., and Coauthors, 2006: The community climate system model version 3 (CCSM3). *J. Climate*, **19**, 2122–2143.

Edwards, J. M., and A. Slingo, 1996: Studies with a flexible new radiation code. I: Choosing a configuration for a large-scale model. *Quart. J. Roy. Meteor. Soc.*, **122**, 689–719.

Friedlingstein, P., and Coauthors, 2006: Climate–Carbon

cycle feedback analysis: Results from the C4MIP model intercomparison. *J. Climate*, **19**, 3337–3353.

Li, J. D., Z. Sun., Y. M. Liu, J. N. Li, W.-C. Wang, and G. X. Wu, 2012: A study on sulfate optical properties and direct radiative forcing using LASG-IAP general circulation model. *Adv. Atmos. Sci.*, **29**(6), 1185–1199, doi: 10.1007/s00376-012-1257-y.

Li, Y. C., and Y. F. Xu, 2012: Uptake and storage of anthropogenic CO_2 in the Pacific Ocean estimated using two modeling approaches. *Adv. Atmos. Sci.*, **29**(4), doi: 10.1007/s00376-012-1170-4.

Lin, P. F., H. L. Liu, and X. H. Zhang, 2007: Sensitivity of the upper ocean temperature and circulation in the equatorial Pacific to solar radiation penetration due to phytoplankton. *Adv. Atmos. Sci.*, **24**, 765–780, doi: 10.1007/s00376-007-0765-7.

Lin, P. F., Y. Q. Yu, and H. L. Liu, 2013: Long-term stability and oceanic mean state simulated by the coupled model FGOALS-s2. *Adv. Atmos. Sci.*, **30**, 175–192, doi: 10.1007/s00376-012-2042-7.

Liu, H. L., Y. Q. Yu, W. Li, and X. H. Zhang, 2004: *Manual for LASG/IAP climate system ocean model* (*LICOM1.0*). Science Press, Beijing, 128pp. (in Chinese)

Liu, Y. M., J. Hu, B. He, Q. Bao, A. M., Duan and G. X. Wu, 2013: Seasonal evolution of the subtropical anticyclones in a climate system model FGOALS-s2. *Adv. Atmos. Sci.*, doi: 10.1007/s00376-012-2154-0.

Lumpkin, R., and K. Speer, 2007: Global ocean meridional overturning. *J. Phys. Oceanogr.*, **37**, 2550–2562.

Meehl, G. A., and T. F. Stocker, 2007: Global climate projections. *Climate Change 2007: The Physical Science Basis*, S. Solomon, et al., Eds., Cambridge University Press, United Kingdom and New York, 996pp.

Mitchell, T. D., and P. Jones, 2005: An improved method of constructing a database of monthly climate observations and associated high-resolution grids. *Int. J. Climatol.* **25**, 693–712.

Oleson, K. W., and Coauthors, 2004: Technical description of the community land model (CLM). NCAR/TN-461+STR, 173pp.

Rayner, N. A., and Coauthors, 2003: Global analyses of sea surface temperature, sea ice, and night marine air temperature since the late nineteenth century. *J. Geophys. Res.*, **108**, 37pp.

Song, X. L., 2005: The evaluation analysis of two kinds of mass-flux cumulus parameterization in climate simulation. Institute of Atmospheric Physics, Chinese Academy of Sciences, Ph.D. dissertation, 158pp. (in Chinese)

Sun, Z., 2011: Improving transmission calculations for Edwards-Slingo radiation scheme using a correlated k-distribution method. *Quart. J. Roy. Meteor. Soc.*, **137**, 2138–2148.

Sun, Z. A., and L. Rikus, 1999a: Improved application of exponential sum fitting transmissions to inhomogeneous atmosphere. *J. Geophys. Res.*, **104**, 6291–6303.

Sun, Z. A., and L. Rikus, 1999b: Parametrization of effective sizes of cirrus-cloud particles and its verification against observations. *Quart. J. Roy. Meteor. Soc.*, **125**, 3037–3055.

Taylor, K. E., R. J. Stouffer, and G. Meehl, 2012: An overview of CMIP5 and the experiment design. *Bull. Amer. Meteor. Soc.*, **93**, 485–498.

Tiedtke, M., 1989: A comprehensive mass flux scheme for cumulus parameterization in large-scale models. *Mon. Wea. Rev.*, **117**, 1779–1800.

IPCC, 2007: Observations: Surface and atmospheric climate change. *Climate Change 2007: The Physical Science Basis*, S. Solomon, et al., Eds., Cambridge University Press, United Kingdom and New York, 996pp.

Wallace, J. M. and D. S. Gutzler, 1981: Teleconnections in the geopotential height field during the Northern Hemisphere winter. *Mon. Wea. Rev.*, **109**, 784–812.

Wang, B., and Q. H. Ding, 2006: Changes in global monsoon precipitation over the past 56 years. *Geophys. Res. Lett.*, **33**, doi: L06711.06711-L06711.06714.

Wang, Z. Z., G. X. Wu, P. Liu, and T. W. Wu, 2005: The development of GOALS/LASG AGCM and its global climatological features in climate simulation I: Influence of horizontal resolution. *Journal of Tropical Meteorology*, **21**, 225–237. (in Chinese)

Wu, F. H., H. L. Liu, W. Li, and X. H. Zhang, 2005: Effects of adjusting vertical resolution on the eastern equatorial Pacific cold tongue. *Acta Oceanologica Sinica*, **24**, 16–27. (in Chinese)

Xiao, C., 2006: Adoption of a two-step shape-preserving advection scheme in an OGCM and its coupled experiment. Ph.D. dissertation, Institute of Atmospheric Physics, Chinese Academy of Sciences, Beijing, 89pp. (in Chinese)

Xie, P. P., and P. A. Arkin, 1997: Global precipitation: A 17-year monthly analysis based on gauge observations, satellite estimates, and numerical model outputs. *Bull. Amer. Meteor. Soc.*, **78**, 2539–2558.

Yang, J., B. Wang and B. Wang, 2008: Anti-correlated intensity change of the quasi-biweekly and 30C̈50-day oscillations over the South China Sea. *Geophys. Res. Lett.*, **35**, L16702, doi: 10.1029/2008GL034449.

Yang, J., B. Wang, B. Wang, and Q. Bao, 2010: Biweekly and 21–30 day variabilities of the subtropical East Asian monsoon over the Lower reach of Yangtze River Basin. *J. Climate*, **23**, 1146–1159.

Yang, J., Q. Bao, X. C. Wang, and T. J. Zhou. 2012: The tropical intraseasonal oscillation in SAMIL coupled and uncoupled general circulation models. *Adv. Atmos. Sci.*, doi: 10.1007/s00376-011-1087-3.

Yu, R. C., and T. J. Zhou, 2004: Impacts of winter-NAO on March cooling trends over subtropical Eurasia continent in the recent half century. *Geophys. Res. Lett.*, **31**, doi: 10.1029/2004GL019814.

Yu, Y. Q., W. P. Zheng, B. Wang, H. L. Liu, and J. P. Liu, 2011: Versions g1.0 and g1.1 of the LASG/IAP flexible global ocean-atmosphere-land system model. *Adv. Atmos. Sci.*, **28**, 99–117, doi: 10.1007/s00376-

010-9112-5.

Zeng, N., H. F. Qian, E. Munoz, and R. Iacono, 2004: How strong is carbon cycle-climate feedback under global warming. *Geophys. Res. Lett.*, 31, doi: 10.1029/2004GL020904.

Zhang, X. H., and X. Z. Liang, 1989: A numerical world ocean general circulation model. *Adv. Atmos. Sci.*, **6**, 44–61.

Zhang, X. H., G. Y. Shi, H. Liu, and Y. Q. Yu, 2000: *IAP Global Ocean-Atmosphere-Land System Model*. Science Press, Beijing, 252pp. (in Chinese)

Zhang, Y., J. M. Wallace, and D. S. Battisti, 1997: ENSO-like interdecadal variability: 1900–93. *J. Climate*, **10**, 1004–1020.

Zhou, T. J., R. C. Yu, Z. Z. Wang, and T. W. Wu, 2005: *Atmospheric Circulation Global Model* (*SAMIL*) *and the Coupled Model* (*FGOALS-s*). Vol. 4, China Meteorological Press, 288pp. (in Chinese)

Zhou, T. J., X. H. Zhang, Y. Q. Yu, R. C. Yu, and S. W. Wang, 2000: The North Atlantic oscillation simulated by versions 2 and 4 of IAP/LASG GOALS Model. *Adv. Atmos. Sci.*, **17**, 601–616.